JACS
JOURNAL OF THE AMERICAN CHEMICAL SOCIETY

Article

pubs.acs.org/JACS

A Discrete Three-Layer Stack Aggregate of a Linear Porphyrin Tetramer: Solution-Phase Structure Elucidation by NMR and X-ray Scattering

Marie Hutin, Johannes K. Sprafke, Barbara Odell, Harry L. Anderson,* and Tim D. W. Claridge*

Department of Chemistry, University of Oxford, Chemistry Research Laboratory, Mansfield Road, Oxford OX1 3TA, United Kingdom

Supporting Information

ABSTRACT: Formation of stacked aggregates can dramatically alter the properties of aromatic π-systems, yet the solution-phase structure elucidation of these aggregates is often impossible because broad distributions of species are formed, giving uninformative spectroscopic data. Here, we show that a butadiyne-linked zinc porphyrin tetramer forms a remarkably well-defined aggregate, consisting of exactly three molecules, in a parallel stacked arrangement (in chloroform at room temperature; concentration 1 mM−0.1 μM). The aggregate has a mass of 14.7 kDa. Unlike most previously reported aggregates, it gives sharp NMR resonances and aggregation is in slow exchange on the NMR time scale. The structure was elucidated using a range of NMR techniques, including diffusion-editing, ^{1}H−^{29}Si HMBC, ^{1}H−^{1}H COSY, TOCSY and NOESY, and ^{1}H−^{13}C edited HSQC spectroscopy. Surprisingly, the ^{1}H−^{1}H COSY spectrum revealed many long-range residual dipolar couplings (RDCs), and detailed analysis of magnetic field-induced ^{1}H−^{13}C RDCs provided further evidence for the structural model. The size and shape of the aggregate is supported by small-angle X-ray scattering (SAXS) data. It adopts a geometry that maximizes van der Waals contact between the porphyrins, while avoiding clashes between side chains. The need for interdigitation of the side chains prevents formation of stacks consisting of more than three layers. Although a detailed analysis has only been carried out for one compound (the tetramer), comparison with the NMR spectra of other oligomers indicates that they form similar three-layer stacks. In all cases, aggregation can be prevented by addition of pyridine, although at low pyridine concentrations, disaggregation takes many hours to reach equilibrium.

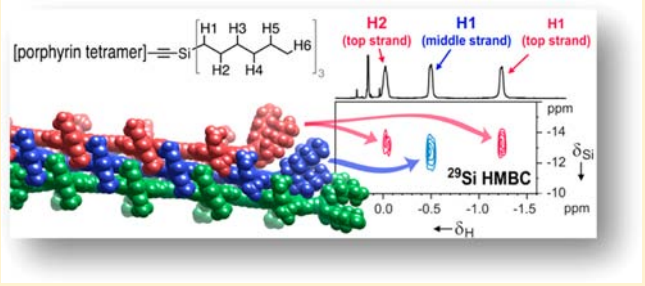

INTRODUCTION

Aggregation is an important, yet poorly understood, property of molecular π-systems.[1] The current lack of understanding of aggregation behavior is a severe problem in the rational design of molecular organic semiconductors for field-effect transistors (FETs)[2] and light emitting diodes (OLEDs).[3] Aggregation is a crucial issue in the design of optical and nonlinear optical materials: often a dye that exhibits excellent optical characteristics in dilute solution cannot be used in thin films because aggregation broadens the absorption spectra or quenches the luminescence, although, in some cases, aggregation can lead to sharp absorption and enhanced fluorescence.[4] Cooperative aggregation processes have attracted great attention for stimuli-responsive materials,[5] while long columnar stack-aggregates exhibit unique optical, electronic and mechanical behavior.[6] One reason why aggregates are poorly understood is that it is often difficult to determine their structures. Compounds which aggregate strongly in solution tend not to form suitable crystals for X-ray analysis, while they typically give broad uninformative solution-phase NMR spectra. Here we present the remarkable case of an aggregate of a porphyrin oligomer which exhibits sharp information-rich NMR spectra, and is in slow exchange with the disaggregated compound on the NMR time scale.[7] A detailed analysis of the spectra reveals that this aggregate consists of three molecules of the porphyrin oligomer, in a π-stacked face-to-face parallel-offset arrangement. Surprisingly, chloroform solutions of this aggregate experience magnetic field-induced alignment and the NMR spectra exhibit residual dipolar coupling (RDC). Analysis of NOE data together with these RDCs provides strong support for our structural model.[8]

Porphyrins and porphyrinoids often aggregate in solution, even in good solvents such as chloroform,[9] and the tendency of chlorophyll molecules to aggregate has been exploited by nature in the evolution of light-harvesting antenna complexes.[10] Simple porphyrins, lacking bulky substituents, generally aggregate in the classic Hunter-Sanders π−π stacked parallel diagonally offset geometry, with the center of one porphyrin above a pyrrole ring of another.[11] However, this arrangement is blocked by the presence of bulky *meso*-substituents, and stacking can be completely prevented by judicious choice of side groups. Another common mode of aggregation involves

Received: June 15, 2013
Published: August 2, 2013

dx.doi.org/10.1021/ja406015r | J. Am. Chem. Soc. 2013, 135, 12798−12807

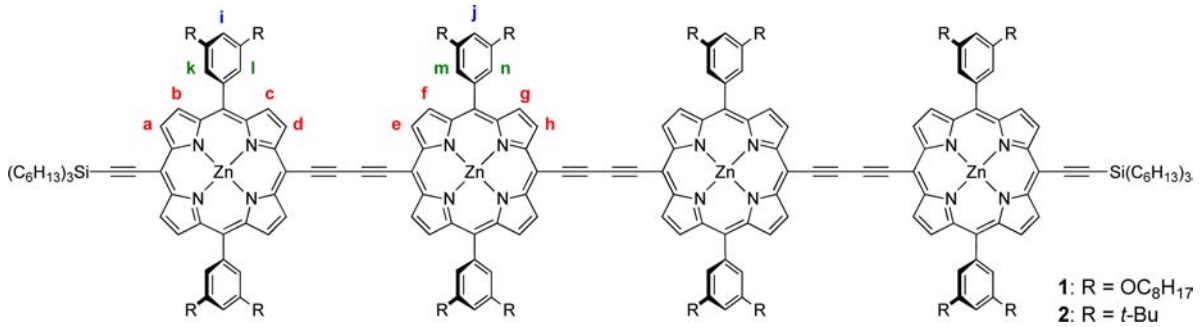

Figure 1. Chemical structure of porphyrin tetramers **1** and **2** showing proton labeling scheme used. When disaggregated, k = l and m = n, but in the aggregate these environments are different.

the coordination of a heteroatom (oxygen or nitrogen) on the periphery of one porphyrin to a metal atom at the center of another porphyrin.[12] At first, when we discovered that porphyrin tetramer **1**, with octyloxy ether side chains, aggregates strongly in noncoordinating solvents, whereas the corresponding compound with *tert*-butyl side chains, **2**, does not aggregate, we concluded that the aggregation must involve oxygen−zinc coordination. However, the results presented here demonstrate that Zn−O coordination does not occur, and that a face-to-face π-stacked aggregate is formed. A surprising feature of this system is the self-assembly of discrete trimolecular aggregates, without any detectable trace of bimolecular or tetra-molecular species. To the best of our knowledge, this is the first report of the formation of discrete trimolecular aggregates, where the number of molecules in the aggregate is determined only by the interdigitation of the side chains.[13] The molecule under investigation is the fully π-conjugated butadiyne-linked porphyrin tetramer **1** (Figure 1).[14] Each porphyrin unit has two aryl substituents bearing 3,5-octyloxy chains to provide solubility in nonpolar solvents, and the ends of the tetramer are capped with trihexylsilyl (THS) groups.

RESULTS AND DISCUSSION

UV−visible Absorption Spectra. Comparison of the UV−vis absorption spectra of the tetramers with OC_8H_{17} side-chains (**1**) and *t*-Bu substituents (**2**)[15] in chloroform indicates that **1** aggregates more strongly than **2** (Figure S2 of the Supporting Information, SI). The shape of both the Soret (400−550 nm) and the Q (650−850 nm) absorption bands of **2** remain almost unchanged when it binds pyridine. In the absence of pyridine, the UV−vis spectrum of **1** in $CHCl_3$ exhibits a substantially broader Soret band than **2**, whereas in the presence of pyridine, the spectra of **1** and **2** are almost identical. The broad split Soret band of the aggregate of **1** is typical of a planarized conjugated porphyrin dimer and can be interpreted as a blue-shifted B_Y band and a red-shifted B_X band.[9a] In general, coordination of pyridine to a zinc porphyrin shifts its absorption bands to longer wavelength by about 10−20 nm, as observed with **2**. In contrast, coordination of pyridine to **1** shifts the absorption maxima to shorter wavelengths, indicating that complexation is associated with a shift in the conformational equilibrium toward more twisted species with weaker π-conjugation. The absorption spectrum of the aggregate must also be influenced by exciton coupling between the tetramer units, but these effects are masked by features originating from changes in conformation. In the absence of pyridine, or other coordinating ligands, the absorption spectrum of **1** in $CHCl_3$ is independent of concentration in the concentration range from 10^{-8} to 10^{-4} M, indicating that the aggregation constant is larger than 10^8 M^{-1}, which is high compared to the aggregation constants reported for other extended π-systems.[1,4f,9] Addition of pyridine causes disaggregation, by coordination to the zinc centers to form the pyridine complex $\mathbf{1}\cdot(\mathbf{py})_4$. At low pyridine concentrations, this disaggregation process is slow, and the equilibrium is not reached within 10 h at 25 °C (Figure S3b of the SI). The reaction is faster at higher pyridine concentrations and addition of 100 equivalents of pyridine results in complete disaggregation in less than 30 min.

NMR Structural Analysis. Insights into the structure of the aggregate of **1** were provided by detailed NMR analyses, which are described below. To clarify the discussions that follow, it is beneficial to present our final model for the structure of the aggregate, before presenting the evidence supporting this model. The structure consists of three porphyrin tetramer units stacked in a parallel offset fashion, in which the zinc atoms sit above the butadiyne linkers ($\mathbf{1}_3$, Figure 2). The 12 zinc

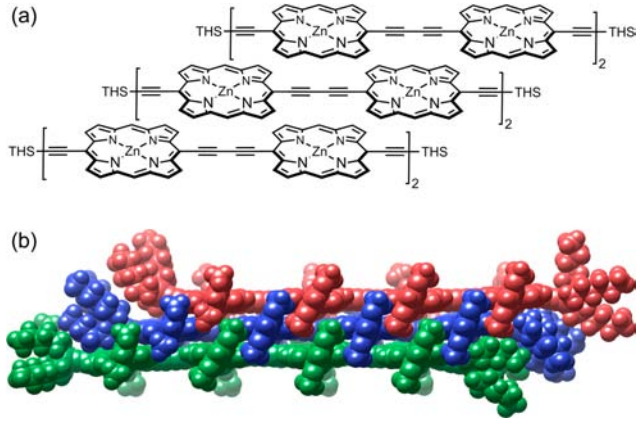

Figure 2. (a) Schematic representation of the triple-strand aggregate $\mathbf{1}_3$, not showing aryl side groups, and (b) calculated molecular model of the $\mathbf{1}_3$ aggregate (with octyloxy side chains replaced by methoxy groups).

atoms lie in a plane which is perpendicular to the planes of the 12 porphyrin macrocycles. This offset arrangement avoids steric clashes of the *meso*-aryl groups, which interdigitate along the length of the aggregate, and allows close contact between the porphyrin strands (3.4−3.5 Å separation). The aryl groups are tilted at an angle of ~60° to the plane of the porphyrin rings and are oriented to minimize steric clash of the octyloxy and the hexylsilyl chains. The point group of the aggregate is C_{2h};

dx.doi.org/10.1021/ja406015r | J. Am. Chem. Soc. 2013, 135, 12798−12807

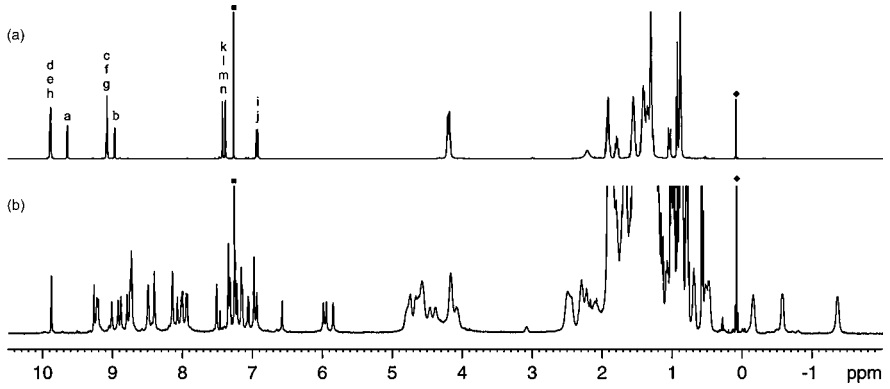

Figure 3. ^{1}H NMR spectra ($CDCl_3$, 500 MHz, 298 K) of (a) tetramer **1**·**(py)**$_4$ in the presence of 1% pyridine-d_5 and (b) as the aggregate $\mathbf{1}_3$. Resonance labeling follows the scheme of Figure 1. (Black squares indicate residual solvent $CHCl_3$ and black diamonds denote trace silicon grease.).

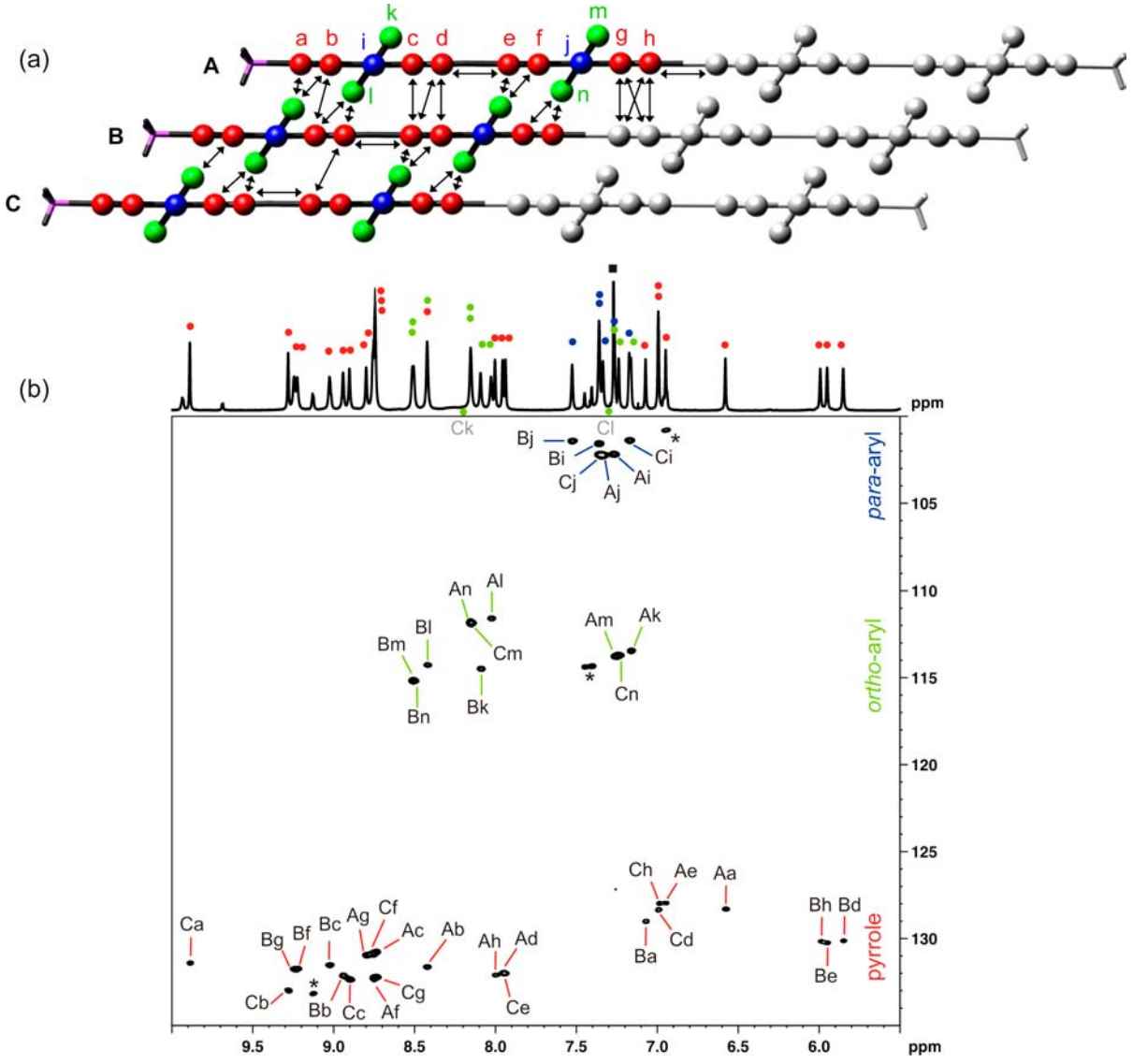

Figure 4. (a) Cartoon representation of the aggregate $\mathbf{1}_3$ illustrating color coding of proton type, with symmetry related positions shaded gray. Key NOE correlations are indicated by black arrows (see Figure S7 of the SI for details). (b) The partial ^{1}H−^{13}C HSQC spectrum of $\mathbf{1}_3$ ($CDCl_3$, 700 MHz, 298 K) showing the aromatic region. Peaks are labeled and color coded according to proton type and the locations of the broad *ortho*-aryl proton resonances (Ck and Cl) discussed in the text are indicated with green circles below the ^{1}H spectrum. Peaks labeled with an asterisk arise from the presence of the disaggregated pyridine adduct **1**·**(py)**$_4$ and the black square identifies the solvent residual peak of $CHCl_3$. The assignments of the Aj and Cj *para*-aryl protons may be interchanged.

dx.doi.org/10.1021/ja406015r | J. Am. Chem. Soc. 2013, 135, 12798−12807

there is a 2-fold rotation axis perpendicular to the mirror plane passing through the 12 zinc centers. Its molecular weight is 14,719 Da. Tetramer **2**, in which the octyloxy side chains are replaced with *tert*-butyl groups, would be unable to form a similar aggregate as these side chains would prevent the interdigitation of the aryl groups and so hinder stacking, consistent with experimental observations.

The ^{1}H NMR spectra of the analogous porphyrin monomer and dimer in $CDCl_3$ (with or without pyridine) are consistent with their symmetry. In the presence of pyridine, tetramer **1** also gives a simple ^{1}H NMR spectrum (Figure 3a). However, in the absence of pyridine, the spectrum of **1** in $CDCl_3$ exhibits a large number of sharp, well-defined, and widely dispersed peaks, in contradiction with the symmetry of an isolated tetramer (Figure 3b). Some of these signals have negative chemical shifts, indicating that parts of the molecule experience strong ring current shielding in the aggregated state. The ^{1}H NMR spectra of aggregates often show broad, poorly resolved peaks.[16] The sharpness of the peaks and the complexity of the ^{1}H NMR spectrum of $\mathbf{1}_3$ in the absence of pyridine indicate a high degree of order in the aggregate and prompted us to analyze its structure in detail.

^{1}H DOSY NMR studies were performed in $CDCl_3$ to determine the size of the aggregates (Figure S4 of the SI). These experiments revealed that the diffusion coefficient of the aggregate $\mathbf{1}_3$ in $CDCl_3$ is similar to that of the ladder complex $\mathbf{1}_2$·**(DABCO)**$_4$, where DABCO is the bidentate ligand 1,4-diazabicyclo[2.2.2]octane.[15] This indicates that the aggregate contains about 2−4 tetramer units, and as will be described below, the NMR spectra of the aggregate are consistent with the stacked triple-stranded structure of Figure 2. In describing the triple-stranded complex, the three tetramer strands of the aggregate shall be referred to as strands A, B, and C, (Figure 4a) with each comprising three classes of aromatic protons: the *β*-pyrrolic protons shown in red (Ha−Hh), the *para*-aryl protons in blue (Hi and Hj) and the *ortho*-aryl protons in green (Hk−Hn). In addition, the two groups of *β*-pyrrolic protons are differentiated as being adjacent to the butadiyne links (Ha, Hd, He, and Hh) or the aryl groups (Hb, Hc, Hf and Hg). Due to the C_{2h} symmetry of the aggregate, only one-half of each molecule gives rise to distinct proton environments which shall be distinguished by three letter codes, e.g., HAd (proton d on strand A).

Through extensive analysis of 2D NMR data described herein, it has been possible to specifically assign each aromatic resonance to a unique proton in the structure, and hence demonstrate consistency with the symmetry requirements of the triple-stranded complex. Thus, through analysis of the ^{1}H spectrum integration and peak distribution in the ^{1}H−^{13}C HSQC (Figure 4b) it was possible to identify 12 unique environments for pairs of *β*-pyrrole protons (a−h, representing 96 protons) and 6 unique environments for the aryl *para*-protons (i and j, representing 24 protons). In the case of the aryl *ortho*-protons, the aromatic rings are prevented from undergoing ring rotation, being locked by the interdigitation, and thus separate resonances are observed for the two *ortho*-positions within each aryl ring (k/l and m/n). This would lead to 12 unique *ortho*-proton environments (representing 48 protons) in the triple-stranded structure, although only 10 environments could be identified in the HSQC spectrum. However, two very broad resonances could be identified beneath the sharper peaks in the ^{1}H spectrum, and we reasoned that these arose from the aryl groups at the terminal end of the more exposed porphyrin (HCk and HCl of strand C in Figure 4a). In this environment, the aryl groups rotate due to reduced steric hindrance in this region, giving rise to exchange-broadened resonances. (These broad peaks were subsequently correlated with the terminal *β*-pyrrole protons HCb through NOE data.) Thus, it is possible to account for the presence of all 168 aromatic protons in the triple-stranded complex. Further consideration of the ^{1}H resonances for the aryl groups indicated the six unique environments for the *para*-aryl protons are quite similar, as evidenced by the clustering of peaks. This would be anticipated since these protons all sit on the outer rim of the triple strand and would be relatively insensitive to the strand stacking. In contrast, and as discussed further below, the *ortho*-aryl proton resonances divide into two regions (Figure 4b), with four (including the broadened resonance of HCl) appearing below 7.5 ppm and eight appearing deshielded above 8.0 ppm (including the corresponding broadened resonance of HCk) correlating with "outside" and "inside" *ortho*-aryl locations within the aggregate, respectively.

The initial realization that the aggregate must comprise three strands arose from the analysis of the aliphatic region of the spectrum, particularly the strongly shielded protons resonating below 0 ppm, which were shown to arise uniquely from the hexylsilyl groups at the termini of the porphyrin strands. Thus, 1D ^{1}H TOCSY spectra suggested these to be C6, rather than C8, alkyl chains and ^{1}H−^{29}Si HMBC spectra definitively proved them to arise from the hexylsilyl groups (Figure 5), which were

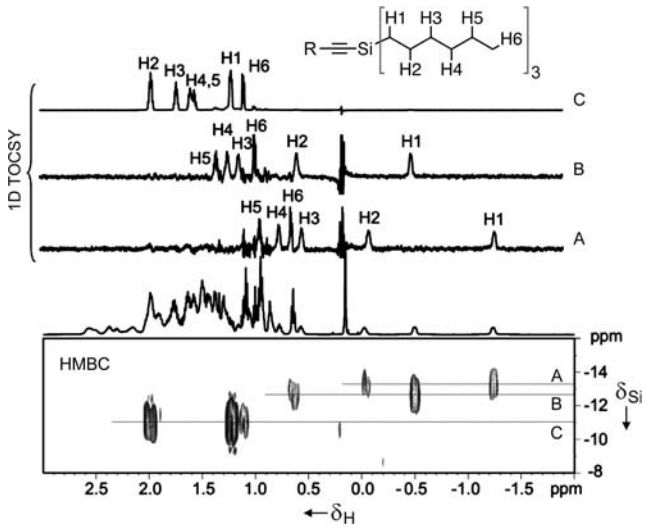

Figure 5. ^{1}H−^{29}Si HMBC ($CDCl_3$, 500 MHz, 328 K) and 1D TOCSY spectra ($CDCl_3$, 700 MHz, 298 K, 150 ms mixing times with H1 as the selected excitation target in each case) identifying the three different silicon environments of strands A, B, and C for the THS groups of $\mathbf{1}_3$. The HMBC spectrum was recorded at elevated temperature as this sharpened the ^{1}H resonances slightly, giving rise to more intense correlations.

further assigned in ^{1}H−^{13}C HSQC spectra (Figure S5 of the SI). These experiments also defined only three separate environments for the hexylsilyl groups and so suggested the possibility of a triple-stranded complex with a central 2-fold rotational symmetry axis. The two alkyl chains experiencing the greatest ring current shielding were subsequently assigned to the termini of strands A and B, both of which reside above an adjacent porphyrin ring. In contrast, the hexylsilyl chains of strand C project from the aggregate and experienced negligible

dx.doi.org/10.1021/ja406015r | J. Am. Chem. Soc. 2013, 135, 12798−12807

Table 1. Summary of the Experimentally Observed $^1H-^{13}C$ Total Splittings ($^1T_{CH} = {}^1J_{CH} + {}^1D_{CH}$), the Scalar $^1J_{CH}$ Couplings and the Residual Dipolar Couplings ($^1D_{CH}$ at 700 MHz) for All *ortho* and *para*-Aryl Protons and *β*-Pyrrole Protons[a]

assignment	δ_H (ppm)	δ_C (ppm)	$^1T_{CH}$700 MHz (Hz)	$^1T_{CH}$ 500 MHz (Hz)	$^1T_{CH}$ 300 MHz (Hz)	$^1J_{CH}$ (Hz)	$^1D_{CH}$ 700 MHz (Hz)	$^1D_{CH,Calc}$ 700 MHz (Hz)
ortho-aryl								
Ak	7.17	113.5	171.7	166.3	162.1	160.1	11.6	11.4
Al	8.02	111.6	168.0	163.9	162.0	160.4	7.6	7.0
Am	7.27	113.8	172.4	166.4	162.0	159.8	12.6	13.0
An	8.16	111.8	168.3	163.7	162.0	160.2	8.1	5.1
Bk	8.10	114.5	168.9	163.9	160.9	159.0	9.9	8.6
Bl	8.43	114.4	167.6	164.3	160.9	159.7	7.9	10.4
Bm	8.52	115.2	167.4	163.7	160.9	159.5	7.9	10.0
Bn	8.51	115.1	167.3	163.7	160.9	159.6	7.7	8.8
Cm	8.15	111.9	168.3	163.7	162.0	160.2	8.1	6.2
Cn	7.24	113.7	171.4	165.7	162.0	159.9	11.5	11.7
para-aryl								
Ai	7.27	102.2	145.1	150.7	153.4	155.5	−10.4	−12.3
Aj or Cj	7.36	102.3	143.4	150.5	153.4	156.1	−12.7	−11.8
Bi	7.36	101.6	145.1	150.9	153.4	155.6	−10.5	−12.6
Bj	7.53	101.4	145.1	150.9	153.4	155.6	−10.5	−12.6
Ci	7.17	101.4	145.0	150.9	153.4	155.7	−10.7	−12.5
Cj or Aj	7.34	102.3	143.4	150.3	153.4	156.0	−12.6	−11.9
β-pyrrole								
Aa	6.65	128.3	166.6	170.0	171.7	173.0	−6.4	−7.3
Ab	8.48	131.6	160.9	166.0	171.7	173.5	−12.6	−12.1
Ac	8.75	130.7	160.3	166.8	171.0	173.4	−13.1	−11.9
Ad	7.96	132.0	168.4	172.2	174.5	175.9	−7.5	−7.3
Ae	6.95	128.0	165.3	169.8	171.8	173.5	−8.2	−6.9
Af	8.76	132.2	160.7	167.5	172.0	174.5	−13.8	−12.0
Ag	8.80	130.9	160.8	167.8	171.0	173.7	−12.9	−11.2
Ah	8.00	132.1	168.4	172.4	174.5	176.0	−7.6	−7.3
Ba	7.14	129.0	166.3	169.9	171.7	173.1	−6.8	−7.4
Bb	8.99	132.2	161.7	166.8	171.0	172.9	−11.2	−11.8
Bc	9.03	131.7	160.0	166.7	172.0	174.5	−14.5	−12.5
Bd	5.86	130.1	166.6	170.3	171.8	173.2	−6.6	−7.2
Be	5.95	130.3	166.8	170.0	171.8	173.0	−6.2	−7.2
Bf	9.23	131.7	161.4	167.1	170.9	173.0	−11.6	−12.1
Bg	9.25	131.7	161.4	166.0	171.0	172.7	−11.3	−12.3
Bh	6.00	130.2	166.8	170.3	171.8	173.1	−6.3	−7.3
Ca	9.94	131.4	166.6	170.3	172.0	173.4	−6.8	−5.1
Cb	9.33	133.0	161.6	166.9	172.0	173.9	−12.3	−12.0
Cc	8.91	132.3	160.4	167.1	171.4	173.9	−13.5	−12.5
Cd	7.00	128.3	165.2	170.0	171.8	173.6	−8.4	−6.9
Ce	7.94	132.0	168.4	172.2	174.5	175.9	−7.5	−7.1
Cf	8.76	130.8	160.4	167.2	171.0	173.6	−13.2	−11.0
Cg	8.74	132.1	160.7	167.5	172.0	174.5	−13.8	−12.7
Ch	6.99	128.0	166.4	170.1	171.8	173.2	−6.8	−7.5

[a]The final column summarizes the back-calculated RDC values derived from the triple-stranded aggregate model structure of Figure 2b. No assignments are given for Ck and Cl as these were broadened and thus hidden (see text) while the assignments for Aj and Cj may be interchanged.

ring current shifts. It was further noted that the resonances of the most shielded alkyl protons (H1, H2) are broadened relative to those arising from the ends of the alkyl chains (H5, H6), suggesting restricted motion for methylene groups of strands A and B that are closer to the center of the complex, with greater local flexibility experienced by the chain ends. Consistent with this, it was observed that moderate heating of the sample to 328 K sharpened the broader resonances of strands A and B.

The site-specific assignment of the remaining porphyrin *β*-pyrrole and aryl protons (Figure 4 and Table 1) was possible from thorough analysis of 2D COSY and NOESY spectra, details of which are given in the SI. Key NOE correlations are indicated in Figure 4a. With these data in hand, it becomes possible to rationalize many of the chemical shift features observed for the aggregate (Figure 4b). Most importantly, the stacked offset geometry places those *β*-pyrrole protons adjacent to the butadiyne linkers (a, d, e, and h) immediately below a pyrrole ring of a porphyrin unit in an adjacent strand, thus substantially shielding the protons, consistent with these resonating below 8.3 ppm (the one exception being the exposed terminal proton HCa at 9.94 ppm). In contrast, the *β*-pyrrole protons adjacent to the aryl units (b, c, f, and g) do not sit below a porphyrin ring and thus experience significantly

dx.doi.org/10.1021/ja406015r | J. Am. Chem. Soc. 2013, 135, 12798−12807

reduced shielding effects. The β-pyrrole protons of lowest chemical shift are HBd, HBe, and HBh which belong to the central strand of the stack and are each adjacent to a butadiyne linker. These are clustered at ~6 ppm, being shielded in excess of 3 ppm relative to the disaggregated $\mathbf{1}\cdot(\mathbf{py})_4$, and are sandwiched directly between the pyrrole rings of adjacent strands A and C, thus experiencing their combined shielding effects. In contrast, protons HAd, HAh, and HCe are clustered displaying the highest protons shifts (~8 ppm) and thus lowest net shielding among the β-pyrrole protons adjacent to butadiyne linkers. It is apparent in the aggregate structure (Figure 4a) that there are no aryl groups from a neighboring strand adjacent to these protons, whereas those β-pyrrole protons with lower shifts all have an aryl ring edge pointing toward them. It was also observed that these three protons exhibit unusually large $^1J_{CH}$ couplings (176 Hz; Table 1) which again appear to reflect their unique positions in the aggregate structure. As noted above, of the *ortho*-aryl protons, HAk, HAm, HCl, and HCn display the lowest chemical shifts which are also most similar to those observed for the *ortho*-aryl protons of the disaggregated tetramer $\mathbf{1}\cdot(\mathbf{py})_4$ (~7.4 ppm). These protons are exposed on the outer faces of the stack and are thus less influenced by ring current effects, whereas all other *ortho*-aryl protons are contained within the core of the aggregate and experience significant deshielding, appearing above 8 ppm. Of these, positions Al, An, and Cm exhibit rather low ^{13}C chemical shifts and are seen to be sandwiched between two neighboring aryl groups (most apparent in Figure 2b) while all other such positions (HBk, HBl, HBm, and HBn) possess only a single, immediately adjacent aryl ring. The triple stack structure also explains the appearance of the few observed *inter*-strand β-pyrrole NOEs, namely HAd-HBe, HBd-HCe, and HAh-HBh (which occurs *across* the symmetry interface). These were relatively weak in NOESY spectra and corresponded to distances of ~3.6 Å in the model, being wholly consistent with the offset geometry proposed.

Finally, further consistency with the proposed model was provided through the subsequent synthesis of the analogous porphyrin trimer, which was observed to aggregate in a similar manner, showing very similar ^{1}H peak dispersion and the characteristic shielded resonances of the terminal silylhexyl chains (Figure S8 of the SI). As anticipated, three pairs of β-pyrrole resonances observed for the tetramer were absent from the spectrum of the shorter trimer, suggesting these tetramer resonances to arise from protons at the midpoint of the tetramer aggregate, corresponding to environments Hg and Hh on the central porphyrins.

Magnetic Field Alignment. During the analysis of the NMR data for the aggregate, a number of unusual spectroscopic features became apparent, as described below, which provide evidence for the magnetic field-induced alignment of the aggregate, although this behavior was not observed for the disaggregated pyridine adduct $\mathbf{1}\cdot(\mathbf{py})_4$. The phenomenon of *medium-induced* molecular alignment of biological macromolecules using bicelles, bacteriophages or gels is a well-established tool in structural biology for refining NMR-derived structures through the use of residual dipolar couplings (RDCs) that are made observable because the media prevents isotropic rotational motion of molecules in solution.[17,18] More recently, molecular alignment has also been explored for the investigation of small molecules, employing strongly aligning media, such as liquid crystals or gels.[19,20] For the triple-stranded aggregate, the observed alignment in chloroform solution is entirely field-induced without the influence of additional media, arising from the anisotropic magnetic susceptibility associated with the complex. Such field induced alignment[8,21] has been reported previously for porphyrins,[8b] paramagnetic complexes,[22] and encapsulated aromatic systems.[8d]

In the present study, molecular alignment was first indicated through the influence of RDCs on the appearance of the conventional 1D and 2D NMR spectra. For example, reproducible ^{1}H−^{1}H COSY correlations were clearly observed that would not be anticipated to arise through scalar (J) couplings for a molecule experiencing isotropic tumbling. These included correlations between aryl protons and octyloxy side chains (conventionally five-bond correlations) and between porphyrin β-pyrrole-protons and the terminal hexylsilyl side chains (conventionally at least an eight-bond correlation; Figure S9 of the SI). We also noticed that the apparent ^{1}H−^{1}H coupling constants change with magnetic field strength, as illustrated in Figure 6. Subsequent to the realization

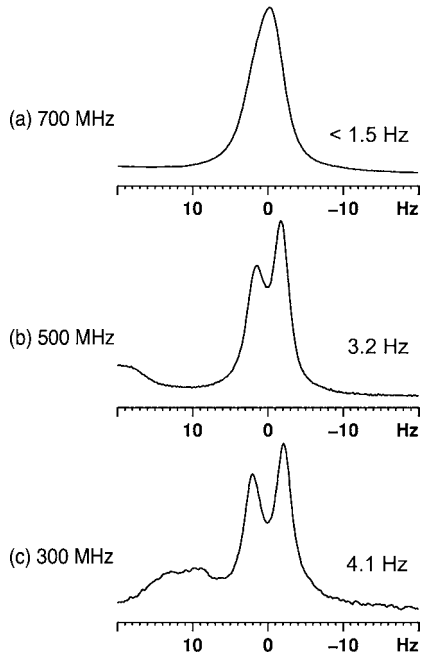

Figure 6. Field-dependence of the splitting for doublet HCa of the ^{1}H spectrum of the tetramer aggregate $\mathbf{1}_3$, illustrating the contribution of residual ^{1}H−^{1}H dipolar couplings ($CDCl_3$, 298 K). For the disaggregated pyridine tetramer adduct $\mathbf{1}\cdot(\mathbf{py})_4$, the observed splitting was 4.1 Hz at all magnetic field strengths.

that the existence of dipolar couplings offered the only feasible explanation for these COSY correlations,[23] we undertook a more systematic study of RDCs through interrogation of heteronuclear one-bond ^{1}H−^{13}C splittings as a function of applied field strength (Figure S10 of the SI). Field-induced alignment increases as the square of the applied magnetic field and observed dipolar couplings would be expected to show a similar dependence. As illustrated in Figure 7, there exists a clear linear correlation between the total observed splittings ($^1T_{CH} = {}^1J_{CH} + {}^1D_{CH}$) and the square of applied field strength, confirming the complex to be field-oriented.[24] An estimate of the authentic $^1J_{CH}$ coupling constants was made through extrapolation to 0 T, revealing the magnitude of the residual dipolar couplings (Table 1). In contrast, no field dependence was observed for the disaggregated pyridine adduct $\mathbf{1}\cdot(\mathbf{py})_4$

dx.doi.org/10.1021/ja406015r | J. Am. Chem. Soc. 2013, 135, 12798−12807

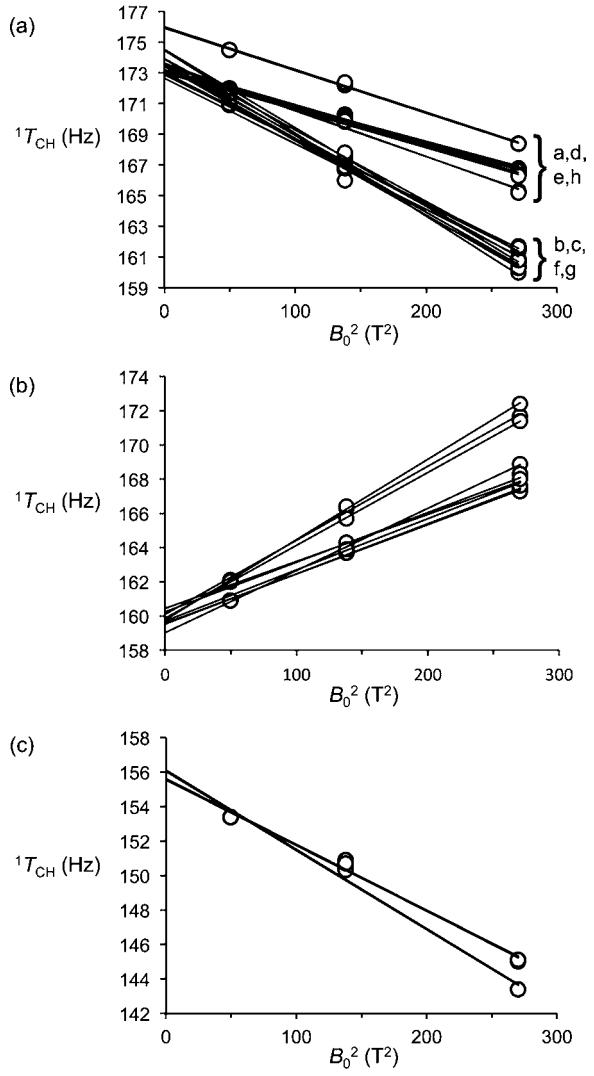

Figure 7. Dependence of the observed ^{1}H−^{13}C total couplings ($^1T_{CH}$) on the square of the applied magnetic field, plotted for (a) β-pyrrole protons, (b) *ortho*-aryl protons, and (c) *para*-aryl protons of the tetramer aggregate. Splittings were recorded from ^{1}H (F_2) traces of ^{13}C-coupled HSQC spectra at ^{1}H frequencies of 700, 500, and 300 MHz.

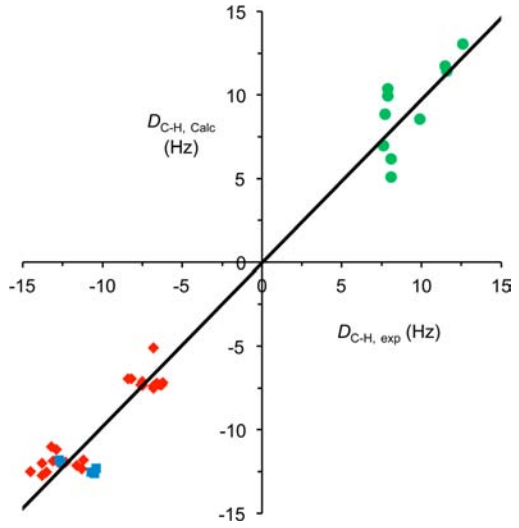

Figure 8. Experimental versus calculated residual dipolar couplings (D_{CH}, Hz) for the tetramer aggregate structure $\mathbf{1}_3$. Proton environments are color coded as for Figure 4: green circles: *ortho*-aryl; blue squares: *para*-aryl; red diamonds: *beta*-pyrrole. The line shows the best fit linear correlation with a slope of 0.977 an R^2 coefficient of 0.976.

(Figure S11 of the SI), suggesting the alignment is significant only for the larger aggregated form of the porphyrin.

From knowledge of sufficient RDCs, it becomes possible to calculate the molecular alignment tensor for a proposed molecular structure and from this back-calculate RDC values for individual ^{13}C−^{1}H pairs in the structure. Good correspondence between all calculated and experimentally determined RDCs helps validate a proposed structure, while significant differences for selected values may suggest local deviations in structure such that orientations of the associated C−H bond vectors do not fit the proposed model. Substantial differences across many values would suggest the model to be a poor representation of the solution structure. Such RDC calculations were performed for the aggregate using the PALES (Prediction of Alignment from Structure) algorithm[25] and the experimental and calculated RDC values for 40 ^{1}H−^{13}C pairs are compared in Figure 8. This shows good agreement between these RDC values with a slope of 0.977 and an R^2 correlation coefficient of 0.976. These results further support the proposed structure comprising three stacked parallel strands with the *meso*-aryl substituents interdigitated and tilted at an angle of ∼60° relative to the plane of the porphyrin rings.

The magnitude of the RDCs observed in the $\mathbf{1}_3$ aggregate are more than an order of magnitude larger than those previously reported for diamagnetic compounds, under magnetic field induced alignment under similar conditions.[8,26] Thus the experimental ^{1}H−^{13}C RDCs ($^1D_{CH}$) for $\mathbf{1}_3$ at a field of 16.4 T (700 MHz) range up to about −12 Hz (Table 1), whereas typical published $^1D_{CH}$ for aromatic compounds are −1.0 Hz for a simple porphyrin monomer[8b] and −0.9 Hz for a metal-coordinated cage complex[8d] (both scaled for a magnetic field of 16.4 T). The data in Table 1 indicate that the $\mathbf{1}_3$ aggregate has a magnetic susceptibility anisotropy of $\Delta\chi = -1.2 \times 10^{-26}$ cm^3 per aggregate unit. The observation that this susceptibility is 12 times greater than that of a typical porphyrin monomer ($\Delta\chi = -9.8 \times 10^{-28}$ cm^3 per molecule)[8a−c] provides strong support for the conclusion that the aggregate consists of 12 porphyrin units in a rigid parallel arrangement.

Small-Angle X-ray Scattering. In order to confirm the size and shape of the $\mathbf{1}_3$ aggregate, we performed solution-phase small-angle X-ray scattering (SAXS) experiments in toluene using synchrotron radiation.[1b,27,28] The electronic pair distribution functions (PDF) obtained from these experiments give a probability distribution for the distance between areas of electron density in the molecule and allow one to obtain structural information by comparison with data simulated from molecular models (Figure 9). The PDF of the disaggregated tetramer acquired in the presence of 1% pyridine perfectly matches the PDF calculated from the molecular model of an isolated molecule of **1**. The three peaks correspond to the three different interporphyrin distances in the molecule. The longest distance peak (41 Å) in the experimental PDF occurs at a slightly shorter distance than in the model, reflecting the flexibility of the tetramer chain in solution. Molecular models for the π-stacked, offset aggregate (as suggested by the NMR data, detailed above) were also calculated based on stacks of two, three and four porphyrin tetramers. The furthest peak in the experimental PDF of the aggregate is not significantly

dx.doi.org/10.1021/ja406015r | J. Am. Chem. Soc. 2013, 135, 12798−12807

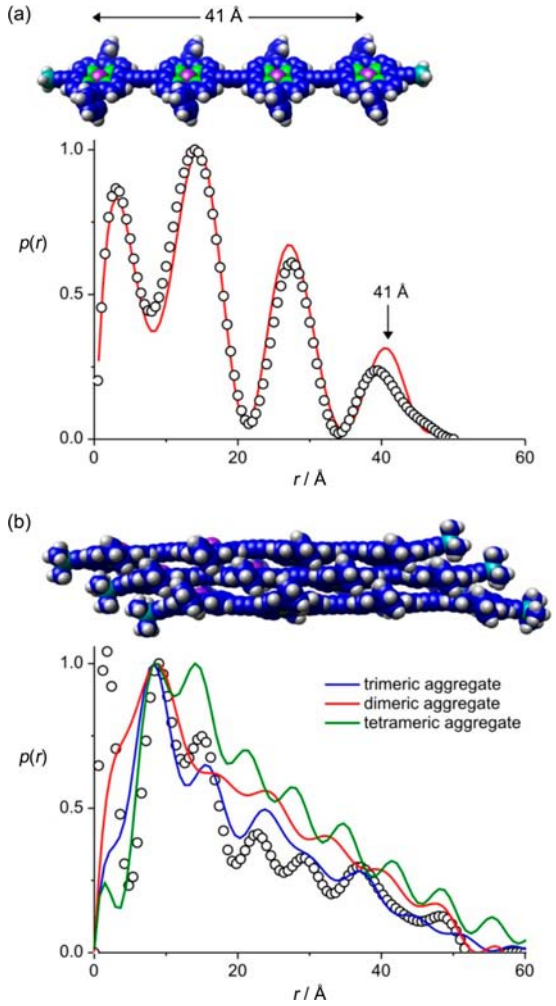

Figure 9. Pair distribution functions obtained from SAXS experiments at 25 °C. (a) **1** in toluene 1% pyridine; (b) **1** in toluene. Experimental data are the black circles and data obtained from molecular models (minimized using the MM+ force field) are lines.

longer (49 Å) than that of the disaggregated tetramer suggesting the formation of a small, well-defined aggregate rather than an extended/polymeric structure. Comparison of the calculated PDFs with the experimental data excludes the formation of an aggregate consisting of four (or more) molecules of **1**, because the longest distance peak at 55 Å is significantly too high and this peak would appear at even greater distances for higher order aggregates. The PDFs simulated from aggregates consisting of two and three tetramer strands are both consistent with the experimental data. These SAXS experiments fully support the triple-strand model for the aggregate, but they provide less precise structural information than the NMR data (number of proton environments, NOEs, and RDCs)

■ CONCLUSIONS

The NMR spectroscopic data presented above show that porphyrin tetramer **1** forms a stable trimolecular aggregate $\mathbf{1}_3$, when dissolved in noncoordinating solvents such as chloroform in the absence of pyridine. This conclusion is supported by diffusion-edited NMR data in $CDCl_3$, and by small-angle X-ray scattering in toluene. Unlike most aggregates, $\mathbf{1}_3$ gives sharp information-rich ^{1}H NMR spectra, and it is in slow exchange with the disaggregated pyridine complex, $\mathbf{1}\cdot(\mathbf{py})_4$ at 298 K. Simulation of the observed RDCs confirms the geometry deduced from the number of observed proton environments, the pattern of NOEs and ring-current induced shifts, while the magnitude of the observed RDCs also confirms that the aggregate is trimolecular. The aggregate has a remarkably well-defined structure, consisting of three parallel offset strands with interdigitated aryl side groups. The interdigitation of these side groups probably favors formation of the trimolecular aggregate over smaller or larger aggregates because the length of the porphyrin-porphyrin repeat unit is just right to accommodate three closely packed aryl substituents. Similar trimolecular aggregates appear to be formed by the analogous porphyrin tetramer without trihexylsilyl end groups (Figure S1 of the SI) and also by the corresponding linear porphyrin trimer (Figure S8 of the SI). It is likely that the same mode of aggregation is adopted by longer linear and cyclic butadiyne-linked porphyrin oligomers,[29] and recent STM studies indicate that similar parallel offset trimolecular aggregates are formed by a 24-porphyrin nanoring on a gold surface (although in this case the aggregates are not exclusively trimolecular and stacks of 2−4 nanorings are detected).[30] In another study, we showed that butadiyne-linked porphyrin oligomers, such as **1**, form stable aggregates at low temperatures (~150 K) in 2-methyltetrahydrofuran. These low-temperature aggregates appear to be different from the $\mathbf{1}_3$ aggregate investigated here, in that they are not destabilized by pyridine, and they give sharp UV−vis-NIR absorption spectra.[31] Understanding the aggregation behavior of porphyrin-based molecular wires is an important step toward being able to control the properties of these materials.

■ EXPERIMENTAL SECTION

NMR data were collected on Bruker AVIII700, AVII500, DRX500, and DPX300 spectrometers operating at 293−298 K unless otherwise stated. 2D NOESY spectra were collected at 500 and 700 MHz with mixing times of up to 250 ms and 1D TOCSY of the hexylsilyl side chains at 500 MHz with DIPSI2 mixing for up to 150 ms. ^{1}H−^{13}C total splitting $^1T_{CH}$ were collected in ^{13}C-coupled HSQC spectra with $1/2T_{CH}$ delays of 2.94 ms ($^1T_{CH}$ = 170 Hz). ^{1}H diffusion NMR data were collected at 500 MHz and 298K using the DSTE-BPP (double stimulated echo-bipolar pair) sequence[32] to avoid any deleterious effects of convection. Diffusion times of 100 ms were used with 5 ms sine-bell encoding gradients with strengths up to 0.25 T/m. Best fitting of RDC data to the model structure was performed with the PALES software according to the protocols described in ref 25.

The synchrotron radiation SAXS data were collected using standard procedures on the I22 beamline at Diamond Light Source (U.K.) equipped with a photon counting detector. The beam was focused onto the detector placed at a distance of 1.25 m from the sample cell. The X-ray wavelength was λ = 1.0 Å and scattering was recorded across the region: $0.03 < q < 1.0$ Å^{-1}. The data were normalized to the intensity of the incident beam; the scattering of the solvent was subtracted using an in-house program. Measurements were performed in either toluene or toluene/1% pyridine at known concentrations (~10^{-4} M) in a solution cell with mica windows (1 mm path length). Simulated scattering curves from molecular models were obtained by fitting to the experimental scattering data using the program CRYSOL.[33] The program GNOM[34] was used to calculate pair distribution functions and radii of gyration from experimental and simulated scattering data. Molecular modeling was carried out using HyperChem (Hypercube Inc.) with the MM+ force field.

dx.doi.org/10.1021/ja406015r | J. Am. Chem. Soc. 2013, 135, 12798−12807

■ ASSOCIATED CONTENT

Supporting Information

Details of UV−vis spectra, NMR spectra, NMR assignments, and SAXS analysis. This material is available free of charge via the Internet at http://pubs.acs.org.

■ AUTHOR INFORMATION

Corresponding Author

tim.claridge@chem.ox.ac.uk; harry.anderson@chem.ox.ac.uk

Notes

The authors declare no competing financial interest.

■ ACKNOWLEDGMENTS

We thank Dr. Jonathan Boyd (University of Oxford) for helpful discussions on residual dipolar couplings; Prof. Christina Thiele and Volker Schmidts (Technische Universitat Darmstadt) for helpful discussions and for replicating our initial RDC alignment calculations; Prof. M. Zweckstetter (Max Planck Institute, Göttingen) for making the PALES program available; Dr. P. Neuhaus (University of Oxford) for preparing some solutions for NMR experiments; and Dr. M. Malfois (Diamond Light Source Ltd.) for help with SAXS experiments. We thank the Swiss National Science Foundation for support and Diamond Light Source for an award of time on beamline I22.

■ REFERENCES

(1) (a) Chen, Z.; Lohr, A.; Saha-Möller, C. R.; Würthner, F. *Chem. Soc. Rev.* **2009**, *38*, 564−584. (b) Wasielewski, M. R. *Acc. Chem. Res.* **2009**, *42*, 1910−1921. (c) Greenland, B. W.; Bird, M. B.; Burattini, S.; Cramer, R.; O'Reilly, R. K.; Patterson, J. P.; Hayes, W.; Cardin, C. J.; Colquhoun, H. M. *Chem. Commun.* **2013**, *29*, 454−456.

(2) (a) Sirringhaus, H.; Brown, P. J.; Friend, R. H.; Nielsen, M. M.; Bechgaard, K.; Langeveld-Voss, B. M. W.; Spiering, A. J. H.; Janssen, R. A. J.; Meijer, E. W.; Herwig, P.; de Leeuw, D. M. *Nature* **1999**, *401*, 685−688.

(3) Weinfurtner, K.-H.; Fujikawa, H.; Tokito, S.; Taga, Y. *Appl. Phys. Lett.* **2000**, *76*, 2502−2504.

(4) (a) Möbius, D. *Adv. Mater.* **1995**, *5*, 437−444. (b) Würthner, F.; Kaiser, T. E.; Saha-Möller, C. R. *Angew. Chem., Int. Ed.* **2011**, *50*, 3376−3410. (c) Chan, J. M. W.; Tischler, J. R.; Kooi, S. E.; Bulović, V.; Swager, T. M. *J. Am. Chem. Soc.* **2009**, *131*, 5659−5666. (d) Deans, R.; Kim, J.; Machacek, M. R.; Swager, T. M. *J. Am. Chem. Soc.* **2000**, *122*, 8565−8566. (e) Hong, Y.; Lam, J. W. Y.; Tang, B. Z. *Chem. Commun.* **2009**, 4332−4353. (f) Lohr, A.; Grüne, M.; Würthner, F. *Chem.—Eur. J.* **2009**, *15*, 3691−3705.

(5) (a) De Greef, T. F. A.; Smulders, M. M. J.; Wolffs, M.; Schenning, A. P. H. J.; Sijbresma, R. P.; Meijer, E. W. *Chem. Rev.* **2009**, *106*, 5687−5754. (b) Smulders, M. M. J.; Nieuwenhuizen, M. M. L.; de Greef, T. F. A.; van der Schoot, P.; Schenning, A. P. H. J.; Meijer, E. W. *Chem.—Eur. J.* **2010**, *16*, 362−367. (c) Mayerhoffer, U.; Würthner, F. *Chem. Sci.* **2012**, *3*, 1215−1220.

(6) (a) Aida, T.; Meijer, E. W.; Stupp, S. I. *Science* **2012**, *335*, 813−817. (b) Percec, V.; Glodde, M.; Bera, T. K.; Miura, Y.; Shiyanovskaya, I.; Singer, K. D.; Balagurusamy, V. S. K.; Heiney, P. A.; Schnell, I.; Rapp, A.; Spiess, H.-W.; Hudson, S. D.; Duan, H. *Nature* **2002**, *419*, 384−387. (c) Hollingworth, J. V.; Richard, A. J.; Vicente, G. H.; Russo, P. S. *Biomacromolecules* **2012**, *13*, 60−72. (d) Kaiser, T. E.; Stepanenko, V.; Würthner, F. *J. Am. Chem. Soc.* **2009**, *131*, 6719−6732. (e) Miyajima, D.; Araoka, F.; Takezoe, H.; Kim, J.; Kato, K.; Takata, M.; Aida, T. *Science* **2012**, *336*, 209−213.

(7) Wu, J.; Fechtenkötter, A.; Gauss, J.; Watson, M. D.; Kastler, M.; Fechtenkötter, C.; Wagner, M.; Müllen, K. *J. Am. Chem. Soc.* **2004**, *126*, 11311−11321.

(8) (a) Lisicki, M. A.; Mishra, P. K.; Bothner-By, A. A.; Lindsey, J. S. *J. Phys. Chem.* **1988**, *92*, 3400−3403. (b) Bothner-By, A. A.; Gayathri, C.; van Zijl, P. C. M.; MacLean, C.; Lai, J.-J.; Smith, K. M. *Magn. Reson. Chem.* **1985**, *23*, 935−938. (c) Bothner-By, A. A.; Dadok, J.; Johnson, T. E.; Lindsey, J. S. *J. Phys. Chem.* **1996**, *100*, 17551−17557. (d) Sato, S.; Morohara, O.; Fujita, D.; Yamaguchi, Y.; Kato, K.; Fujita, M. *J. Am. Chem. Soc.* **2010**, *132*, 3670−3671. (e) Sahu, S. C.; Simplaceanu, V.; Gong, Q.; Ho, N. T.; Glushka, J. G.; Prestegard, J. H.; Ho, C. *J. Am. Chem. Soc.* **2006**, *128*, 6290−6291.

(9) (a) Anderson, H. L. *Inorg. Chem.* **1994**, *33*, 972−981. (b) Lash, T. D.; Gandhi, V. *J. Org. Chem.* **2000**, *65*, 8020−8026. (c) García-Frutos, E. M.; Fernández-Lázaro, F.; Maya, E. M.; Vázquez, P.; Torres, T. *J. Org. Chem.* **2000**, *65*, 6841−6846. (d) Hiroto, S.; Osuka, A. *J. Org. Chem.* **2005**, *70*, 4054−4058. (e) Mysliwiec, D.; Donnio, B.; Chmielewski, P. J.; Heinrich, B.; Stepien, M. *J. Am. Chem. Soc.* **2012**, *134*, 4822−4833.

(10) (a) Cogdell, R. J.; Gall, A.; Köhler, J. *Q. Rev. Biophys.* **2006**, *39*, 227−324. (b) Oostergetel, G. T.; van Amerongen, H.; Boekema, E. J. *Photosynth. Res.* **2010**, *104*, 245−255.

(11) Hunter, C. A.; Sanders, J. K. M. *J. Am. Chem. Soc.* **1990**, *112*, 5525−5534.

(12) (a) Balaban, T. S. *Acc. Chem. Res.* **2005**, *38*, 612−623. (b) Kamada, T.; Aratani, N.; Ikeda, T.; Shibata, N.; Higuchi, Y.; Wakamiya, A.; Yamaguchi, S.; Kim, K. S.; Yoon, Z. S.; Kim, D.; Osuka, A. *J. Am. Chem. Soc.* **2006**, *128*, 7670−7678. (c) Haycock, R. A.; Hunter, C. A.; James, D. A.; Michelsen, U.; Sutton, L. R. *Org. Lett.* **2000**, *2*, 2435−2438. (d) Fujisawa, K.; Sakate, A.; Hirota, S.; Kobuke, Y. *Chem.—Eur. J.* **2008**, *14*, 10735−10744.

(13) (a) Klosterman, J. K.; Yamauchi, Y.; Fujita, M. *Chem. Soc. Rev.* **2009**, *38*, 1714−1725. (b) Ono, K.; Yoshizawa, M.; Kato, T.; Fujita, M. *Chem. Commun.* **2008**, 2328−2330. (c) Lohr, A.; Uemura, S.; Würthner, F. *Angew. Chem., Int. Ed.* **2009**, *48*, 6165−6186.

(14) Drobizhev, M.; Stepanenko, Y.; Rebane, A.; Wilson, C. J.; Screen, T. E. O. S.; Anderson, H. L. *J. Am. Chem. Soc.* **2006**, *128*, 12432−12433.

(15) (a) Taylor, P. N.; Huuskonen, J.; Rumbles, G.; Aplin, R. T.; Williams, E.; Anderson, H. L. *Chem. Commun.* **1998**, 909−910. (b) Taylor, P. N.; Anderson, H. L. *J. Am. Chem. Soc.* **1999**, *121*, 11538−11545.

(16) Abraham, R. J.; Rowan, A. E.; Mansfield, K. E.; Smith, K. M. *J. Chem. Soc., Perkin Trans.* **1991**, 515−521.

(17) Prestegard, J. H.; Bougault, C. M.; Kishore, A. I. *Chem. Rev.* **2004**, *104*, 3519−3540.

(18) Hu, W.; Wang, L. *Ann. R. NMR S.* **2006**, *58*, 231−303.

(19) Boettcher, B.; Thiele, C. M. Stereochemistry of Molecules Determined from Residual Dipolar Couplings. In *Encyclopedia of NMR*; Harris, R. K., Wasylishen, R. E., Eds.; Wiley: New York, 2012; Vol. *8*, pp 4736−4747.

(20) (a) Thiele, C. M. *Eur. J. Org. Chem.* **2008**, 5673−5685. (b) Thiele, C. M. *Concepts Magn. Reson.* **2007**, *30A*, 65−80.

(21) Bothner-By, A. A. Magnetic Field Induced Alignment of Molecules. In *Encyclopedia of NMR*; Grant, D. M., Harris, R. K., Eds.; Wiley: New York, 1996; pp 2932−2938.

(22) Bothner-By, A. A.; Domaille, P. J.; Gayathri, C. *J. Am. Chem. Soc.* **1981**, *103*, 5602−5603.

(23) Bolon, P. J.; Prestegard, J. H. *J. Am. Chem. Soc.* **1998**, *120*, 9366−9367.

(24) Here we define the RDC using the equation $T = J + D$, where T is the total coupling constant, J is the scalar coupling, and D is the dipolar coupling. Some authors use the definition $T = J + 2D$. The choice of definition makes no difference to the analysis, other than changing the magnitude of D by a factor of 2.

(25) Zweckstetter, M. *Nat. Protoc.* **2008**, *3*, 679−690.

(26) Larger RDCs are observed in paramagnetic compounds; see for example ref 22 and Kruck, M.; Wadepohl, H.; Enders, M.; Gade, L. H. *Chem.—Eur. J.* **2013**, *19*, 1599−1606.

(27) Tiede, D. M.; Zhang, R.; Chen, L. X.; Yu, L.; Lindsey, J. S. *J. Am. Chem. Soc.* **2004**, *126*, 14054−14062.

(28) The ^{1}H NMR spectra of **1** in d_8-toluene and d_1-chloroform are nearly identical, suggesting formation of the same type of aggregate in both solvents.

(29) O'Sullivan, M. C.; Sprafke, J. K.; Kondratuk, D. V.; Rinfray, C.; Claridge, T. D. W.; Saywell, A.; Blunt, M. O.; O'Shea, J. N.; Beton, P. H.; Malfois, M.; Anderson, H. L. *Nature* **2011**, *469*, 72−75.
(30) Svatek, S. A.; Perdigao, L. M. A.; Stannard, A.; Wieland, M.; Kondratuk, D. V.; Anderson, H. L.; O'Shea, J. N.; Beton, P. H. *Nano Lett.* **2013**, *13*, 3391−3395.
(31) Kärnbratt, J.; Gilbert, M.; Sprafke, J. K.; Anderson, H. L.; Albinsson, B. *J. Phys. Chem. C* **2012**, *116*, 19630−19635..
(32) Jerschow, A.; Müller, N. *J. Magn. Reson.* **1997**, *125*, 372−375.
(33) Svergun, D. I.; Berbato, C.; Koch, M. H. J. *J. Appl. Crystallogr.* **1995**, *28*, 768−773.
(34) Svergun, D. I. *J. Appl. Crystallogr.* **1992**, *25*, 495−503.